5-1-2022

Low-metallicity globular clusters in the low-mass isolated spiral galaxy NGC 2403

Duncan A. Forbes
Swinburne University of Technology

Anna Ferré-Mateu
Swinburne University of Technology

Jonah S. Gannon
Swinburne University of Technology

Aaron J. Romanowsky
San Jose State University, aaron.romanowsky@sjsu.edu

Jeffrey L. Carlin
Rubin Observatory Project Office

See next page for additional authors

Recommended Citation

Duncan A. Forbes, Anna Ferré-Mateu, Jonah S. Gannon, Aaron J. Romanowsky, Jeffrey L. Carlin, Jean P. Brodie, and Jacob Day. "Low-metallicity globular clusters in the low-mass isolated spiral galaxy NGC 2403" *Monthly Notices of the Royal Astronomical Society* (2022): 802-810. https://doi.org/10.1093/mnras/stac503

Monthly Notices of the ROYAL ASTRONOMICAL SOCIETY

MNRAS **512,** 802–810 (2022) https://doi.org/10.1093/mnras/stac503
Advance Access publication 2022 February 25

Low-metallicity globular clusters in the low-mass isolated spiral galaxy NGC 2403

Duncan A. Forbes,[1]★ Anna Ferré-Mateu,[1,2] Jonah S. Gannon,[1] Aaron J. Romanowsky,[3,4,5] Jeffrey L. Carlin,[6] Jean P. Brodie[1,4] and Jacob Day[3]

[1]*Centre for Astrophysics & Supercomputing, Swinburne University of Technology, Hawthorn VIC 3122, Australia*
[2]*Instituto Astrofisica de Canarias, Av. Via Lactea s/n, E-38205 La Laguna, Spain*
[3]*Department of Physics and Astronomy, San José State University, San José, CA 95192, USA*
[4]*University of California Observatories, 1156 High St., Santa Cruz, CA 95064, USA*
[5]*Department of Astronomy and Astrophysics, University of California, Santa Cruz, CA 95064, USA*
[6]*NSF's NOIRLab/Rubin Observatory Project Office, 950 North Cherry Avenue, Tucson, AZ 85719, USA*

Accepted 2022 February 18. Received 2022 February 17; in original form 2021 December 15

ABSTRACT

The globular cluster (GC) systems of low-mass late-type galaxies, such as NGC 2403, have been poorly studied to date. As a low mass galaxy ($M_* = 7 \times 10^9\,M_\odot$), cosmological simulations predict NGC 2403 to contain few, if any, accreted GCs. It is also isolated, with a remarkably undisturbed HI disc. Based on candidates from the literature, Sloan Digital Sky Survey and Hyper Suprime-Cam imaging, we selected several GCs for follow-up spectroscopy using the Keck Cosmic Web Imager. From their radial velocities and other properties, we identify eight bona-fide GCs associated with either the inner halo or the disc of this bulgeless galaxy. A stellar population analysis suggests a wide range of GC ages from shortly after the big bang until the present day. We find all of the old GCs to be metal-poor with [Fe/H] ≤ -1. The age–metallicity relation for the observed GCs suggests that they were formed over many Gyr from gas with a low effective yield, similar to that observed in the SMC. Outflows of enriched material may have contributed to the low yield. With a total system of ∼50 GCs expected, our study is the first step in fully mapping the star cluster history of NGC 2403 in both space and time.

Key words: galaxies: evolution – galaxies: individual: NGC 2403 – galaxies: star clusters.

1 INTRODUCTION

The globular cluster (GC) systems of galaxies is an area of active research [see review by Forbes et al. (2018) and references therein]. This is particularly true for low-mass galaxies, which have relatively poor GC systems compared to giant galaxies with their populous GC systems. While the Local Group contains some well-known low mass galaxies with modest GC systems, such as M33, the LMC, and the SMC, the study of their GC systems is in some ways complicated by their proximity. In the case of M33, radial velocities of its GCs ($\sim -180\,km\,s^{-1}$) overlap with high-velocity stars of the Milky Way; the recent work of Larsen et al. (2021) found that several claimed GCs, in previous studies of M33, are actually foreground Milky Way stars. The Magellanic Clouds are, of course, in the process of merging with the Milky Way, and it has been speculated for some time that they may have 'lost' GCs to our Galaxy (Lynden-Bell & Lynden-Bell 1995). Thus, we need to look further afield to improve our understanding of the GC systems of such low mass galaxies.

While GC systems, in general, include both *in situ* and *ex situ* (accreted) formed GCs (Forbes & Remus 2018), low mass galaxies are expected to be dominated by *in situ* formed GCs, e.g. Oser et al. (2010) and Remus & Forbes (2021). In particular, galaxies with a total halo mass of $M_h < 10^{11}\,M_\odot$ are expected to be dominated by *in situ* formed GCs (Choksi & Gnedin 2019). This is in contrast to massive galaxies like the Milky Way, the haloes of which are dominated by the accreted GCs of disrupted dwarf galaxies (Forbes 2020).

NGC 2403 is a low mass ($M_V = -19.5$, $M_* = 7 \times 10^9\,M_\odot$), late-type (Scd) spiral galaxy in the outskirts of the M81 group at a distance of 3.2 Mpc (Carlin et al. 2016). It may be infalling for the first time into the M81 group (Williams et al. 2013), with M81 itself lying ∼1 Mpc away. It has a satellite galaxy DDO 44 ($M_V = -12.5$), and recently a smaller dwarf, called MADCASH-1 ($M_V = -7.7$), was discovered by (Carlin et al. 2016). Although DDO 44 shows signs of interacting Carlin et al. (2019), NGC 2403 itself reveals a remarkably undisturbed HI disc (de Blok et al. 2008; Williams et al. 2013). This, and its relative isolation, suggests it is a galaxy that has not undergone a strong tidal interaction nor experienced ram pressure stripping. Although bulgeless, it does host a nuclear star cluster (Lira et al. 2007), and it reveals an extended stellar structure at large radii, which is either an extension of the thick disc or the presence of a faint stellar halo (Barker et al. 2012). It is also an important Cepheid variable calibrator galaxy (Saha et al. 2006).

NGC 2403 has some global properties similar to those of the bulgeless Local Group galaxy M33 (Scd, $M_V = -19.4$). M33 contains a large population of intermediate-age star clusters, particularly at large galactocentric radii (Chandar et al. 2002; Davidge 2003; San Roman, Sarajedini & Aparicio 2010; Fan & de Grijs 2014), with 85 per cent of them kinematically associated with the inner halo and 15 per cent

★ E-mail: dforbes@swin.edu.au

associated with the disc (Chandar et al. 2002). Chandar et al. (2002) found that the inner halo GCs in M33 reveal a significant age spread when compared to those of the Milky Way. A key difference is that M33 has signatures of an *inner* stellar halo but not an *outer* one (Gilbert et al. 2022). This may indicate a relatively small contribution from accreted dwarf galaxies in M33's assembly history. In this context, we note at least one halo GC (HM33-B) which Larsen et al. (2021) argued was accreted on the basis of its anomalous chemical signature.

The GC system of NGC 2403 has been poorly studied to date with very little work on it since the photographic plate study of Battistini et al. (1984). In this work, they identified eight candidates as having colours typical of GCs, six star clusters with bluer colours, and five with redder colours than typical Milky Way GCs. Davidge (2007) also identified another half dozen GC candidates in their infrared imaging and estimated their sizes. NGC 2403 does not appear in the catalogue of Harris, Harris & Alessi (2013) listing galaxies with known GC systems (it lists M33 to have a total of 50 GCs) and its total number of GCs is unknown. Based on its total halo mass of $2–3 \times 10^{11}\,M_{\odot}$ (Li et al. 2020), and the relation of Burkert & Forbes (2020), we predict a total GC system of 40–50 members. Based on a typical GC specific frequency for spiral galaxies, over a range of luminosity, of $S_N \sim 1$ (see Lomelí-Núñez et al. 2022), around 60 GCs are expected. As well as having an undefined number of GCs, we are unaware of any published high-quality spectra for confirmed GCs in this nearby galaxy. Thus, the fraction of disc versus halo GCs and whether its halo GCs resemble those of old halo GCs of the Milky Way, or its younger accreted GCs are unknown. The AMR of NGC 2403's GC system, which potentially holds important clues on the galaxy's assembly history, is currently undefined.

Here, we obtain Keck Cosmic Web Imager (KCWI) spectra for nine GC candidates around NGC 240, finding seven to be confirmed GCs. Along with one other GC in NGC 2403 observed using HIRES on the Keck telescope, bringing the total to eight, we discuss their stellar population properties and compare them to those of SMC/LMC, M33, and the Milky Way. At a distance of 3.2 Mpc (Davidge 2003), 1 arcsec corresponds to 15 pc.

2 GLOBULAR CLUSTER CANDIDATES

Our GC candidates for follow-up spectroscopy have been taken from the literature and supplemented by our own data.

2.1 Literature candidates

From Battistini et al. (1984), we include their objects C1, C4, F1, and F16, and from Davidge (2007), we include D2 and D6. According to Davidge (2007), several GC candidates are partially resolved in their near-IR imaging. They measured extended sizes for D2, D6, F1, F16, and F46. The candidates C1, C4, F16, and F46 are clearly resolved GCs in archival *Hubble Space Telescope Advanced Camera for Surveys* (*HST*/ACS) imaging. We have estimated the effective radius of each of these GCs after subtracting in quadrature the ACS point spread function (based on several; stars in the image). Our radii are listed in Table 1, with F46 from Larsen et al. (2021). While we find a similar size for F16 (2.2 versus 2.7 pc), we can rule out F46 having a size of 10.4 pc, as found by Davidge (2007), based on the ACS imaging. For D2, they estimated a small but extended size of 1.8 pc. We also examined the other candidates listed in Battistini et al. (1984) with available *HST*/ACS imaging but concluded that they are unlikely to be GCs.

Table 1. NGC 2403 GC Candidate Properties.

ID	g (mag)	$g-i$ (mag)	Source	R_p (arcmin)	Size (pc)
C1	19.1	0.15	PS	5.3	3.5
C4	18.2	0.91	DR15	5.3	2.0
D2	18.0	0.68	DR15	8.6	–
D6	19.3	0.95	DR7	14.3	3.6
F1	19.1	0.88	DR7	12.4	5.0
F16	19.5	1.01	DR15	7.9	2.2
JD1	19.0	0.81	DR7	6.7	–
JD2	19.8	0.86	DR15	80	–
JC15	19.8	1.04	HSC	4.2	–
F46	18.3	0.85	DR15	5.0	4.4

Note. Source of photometry, i.e. PanSTARRS, SDSS or Hyper Suprime-Cam (HSC) imaging. R_p is the projected radius from the centre of NGC 2403 (JD2 lies close to DDO 44), with 1 arcmin equivalent to 900 pc. Sizes for D6, F1 are from Davidge (2007), C1, C4, and F16 from this work and F46 from L21.

2.2 New candidates

We used the characteristics of the candidates from Battistini et al. (1984) and Davidge (2007) to help select additional GC candidates for spectroscopic follow-up. In particular, using SDSS DR7, we searched for slightly resolved objects with r-band Petrosian radius < 2 arcsec, i-band magnitude in the range $17 < i < 19$, colour in the range $0.7 < g - i < 1.1$ and $2.0 < u - z < 3.5$. Two of these candidates were targeted for follow-up spectroscopy, which are named JD1 and JD2.

In the case of JD2, it was not selected to be a GC candidate of NGC 2403 as it lies at a projected distance of ∼75 kpc (and hence greater in physical distance), but it does lie near the dwarf satellite galaxy DDO 44 and might be associated with it (given its mass, a couple of GCs might be expected).

We selected further candidates from imaging data obtained with HSC on the Subaru 8.2-m telescope. These data were gathered as part of the Magellanic Analogues Dwarf Companions and Stellar Haloes (MADCASH) survey, a deep, wide-area search for dwarf satellites of nearby Magellanic Cloud analogues. In addition to the deep exposures of NGC 2403 first presented in Carlin et al. (2016), short (30 s) exposures on each field were also taken to prevent bright GC candidates from saturating. Here, we use these g and i band images taken on 2016 February 9, with seeing of 0.89 and 0.59 arcsec, respectively. After combining the g and i band source catalogues, we matched them to *Gaia* EDR3 (Gaia Collaboration et al. 2016, 2021), selecting the best match within 1 arcsec of each source. We then selected all objects with magnitudes $17 < i < 20.5$, colours $0.5 < (g - i) < 1.3$, and at least four′ from the centre of NGC 2403 (to avoid the most crowded regions of the images). We further removed all objects whose *Gaia* proper motions or parallaxes are measured with $>3\sigma$ significance, as GCs at ∼3 Mpc distances should not have measurable proper motions or parallaxes.

After these initial selection criteria, we explored aperture magnitudes from the HSC data and quality parameters from *Gaia* that are known to efficiently select extended objects. Because we have a sample of known NGC 2403 GCs, we can confirm that any selection criteria we implement effectively select known GCs. Fig. 1 shows the difference between the HSC i band magnitudes measured in apertures of 3-pixel and 12-pixel radii, which we label $i_3 - i_{12}$, as a function of PSF magnitude. Objects that are very extended (i.e. galaxies) will have a lot of flux beyond their 3-pixel radius, and thus have high

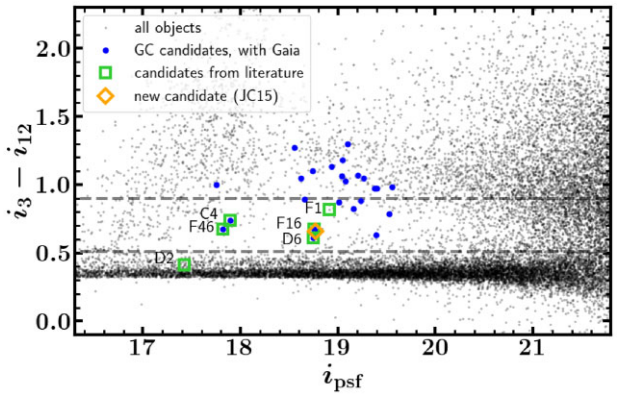

Figure 1. Difference between the i band magnitudes measured on a 30s HSC exposure of NGC 2403 with 3-pixel and 12-pixel apertures, $i_3 - i_{12}$, as a function of the i band PSF magnitude. Point sources occupy the locus at $i_3 - i_{12} \sim 0.35$. More extended objects containing excess flux (relative to the PSF) exhibit larger $i_3 - i_{12}$ values, with those between 0.5 and 0.9 (dashed lines) the best candidates for GCs. We highlight as blue dots the two dozen candidate GCs selected based on all of our criteria, open green squares highlight the six candidate GCs with matches to our HSC catalogue, and the orange diamond highlights the new candidate, JC15, that we followed up spectroscopically (see section 2.2).

values of $i_3 - i_{12}$, while stars should have a small amount of flux beyond a 3-pixel radius, which will be primarily determined by the extendedness of the PSF (and thus roughly the same for all stars). The locus of stars is at $i_3 - i_{12} \sim 0.35$ in Fig. 1. Extended galaxies will be well above this locus, while GCs, which are only slightly extended, will have intermediate flux ratios in this figure.

We note that three candidates do not appear in Fig. 1. They are JD1, which is undetected because it lies in a crowded region of the NGC 2403 disc; JD2, which is beyond the HSC field of view; and F1 as it does not have reliable measurements from *Gaia* (it none the less appears extended according to its measured $i_3 - i_{12}$ value). Candidate D2 has flux ratios in this figure consistent with being a point source, and also a large measured proper motion and is thus likely a foreground star.

Fig. 2 displays the *Gaia* parameters 'astrometric excess noise' (AEN) and 'BP/RP excess', which have been shown by Hughes et al. (2021) to effectively select objects around Cen A that are slightly more extended than the PSF (i.e. candidate GCs), as a function of *Gaia* G magnitude. We overlay and adopt the curves from equations (1) and (2) by Hughes et al. (2021) to separate candidate extended objects from point-like sources.

While this selection yields two dozen candidates, upon visual inspection, we found many of these are obvious background galaxies. Additional work is therefore required to create a comprehensive list, over the entire luminosity function and spatially, of the 50 plus GC candidates expected around NGC 2403.

For the best candidate, which we named JC15, we have obtained a spectrum (see below). JC15 lies close to the confirmed GCs D6 and F16 in the selection figures. Most importantly, JC15 shows signs of extendedness in $i_3 - i_{12}$ but does not have extremely large flux ratios. It appears round in the i band HSC images, with some hints of semi-resolved faint stars at the outskirts.

2.3 Candidates for follow-up spectroscopy

Our final sample of GC candidates for which we obtained spectra is given in Table 1. It lists the g band magnitude and $g-i$ colour taken

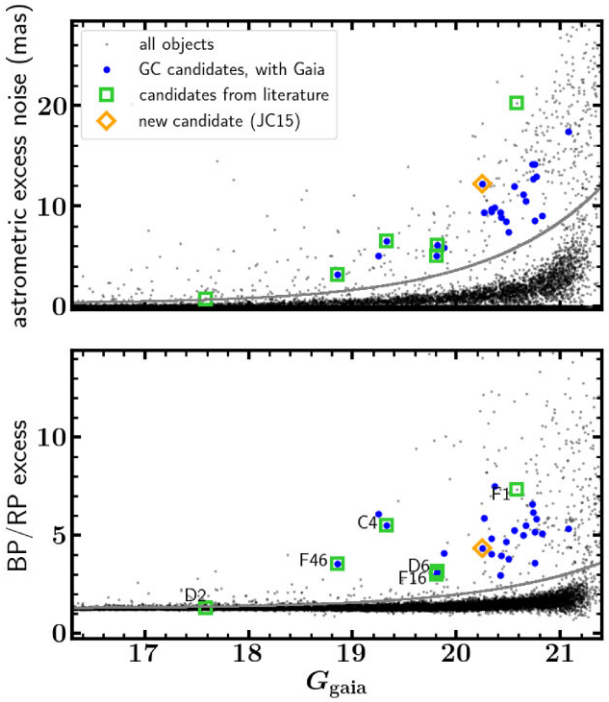

Figure 2. *Gaia* parameters 'AEN' (upper panel) and 'BP/RP excess' (lower panel) as a function of *Gaia* G magnitudes for objects in our HSC imaging. The curves in each panel are the GC candidate selection criteria derived by Hughes et al. (2021) to select Cen A clusters. Symbols are as in Fig. 1.

from SDSS or HSC imaging. The quoted colours are not corrected for Galactic extinction nor internal extinction within NGC 2403. Based on their projected positions on the galaxy disc, JC15 may experience the most internal extinction (it is the reddest object) and D6 the least. We also include in Table 1 (and subsequent tables) the confirmed GC F46. This Battistini et al. (1984) GC candidate, was subsequently confirmed by Larsen et al. (2021) (hereafter L21) using the HIRES instrument at the Keck Observatory.

Fig. 3 shows an image of NGC 2403 with the locations of our GC candidates indicated. Other than JD2, all of our GC candidates follow a flattened disc structure along the major axis. Given the lack of a bulge in NGC 2403, we expect confirmed GCs to be associated with either the disc or the inner halo. In Fig. A1, we show a montage of SDSS, or if available , *HST*, 'postage stamp' images of each GC candidate (including F46 by L21).

3 DATA

GC candidates were observed using the KCWI imager slicer (Morrissey et al. 2018) on the Keck II telescope over several different nights under programmes W140, U216, W024, and N195. In particular, they are D2 (2019 October 29), C4, D6, JD2 (2020 February 16), JC15 (2021 October 4), and F1, F16, JD1, C1 (2022 January 28).

Exposure times ranged from 10 to 40 mins under 1–2 arcsec seeing conditions. We used the medium field-of-view and the BH3 grating (with a spectral resolution $R = 9000$) for C4, D2, D6, JD2. For C1, F1, F16, and JD1, we used the large field-of-view and the BL grating ($R = 900$). Standard stars were observed in the same setups as the target objects. Some lower S/N spectra were also obtained for some of these candidates, but they are not used in this current work.

The data were processed using the standard KCWI data reduction pipeline. We took the non-sky subtracted, standard star calibrated

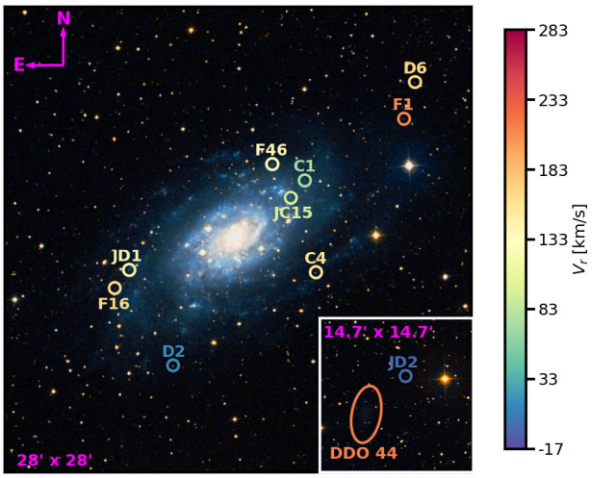

Figure 3. A 28×28 arcmin^2 colour SDSS image of NGC 2403 taken from wikisky. The GC candidates studied in this work are indicated via open circles. They are labelled appropriately and colour coded by their recession velocity (RV). We note that NGC 2403 has an RV of 133 km s^{-1} and the receding side of the galaxy stellar/HI disc (i.e. higher RVs) is the SE side. A 14.7×14.7 arcmin^2 inlay is included to indicate the position of JD2, which is $\sim$1.38° North-North-West of NGC 2403 near the dwarf galaxy DDO 44. At 3.2 Mpc, 1 arcmin = 0.93 kpc. We find D2 and JD2 to be foreground stars.

Table 2. NGC 2403 GC Candidate Spectroscopic Observations.

ID	RA (2000)	Dec. (J2000)	RV (km s^{-1})	S/N	Notes
C1	07:36:10.40	+65:39:35.0	72	58	Disc
C4	07:36:04.43	+65:33:59.8	158	62	Disc
D2	07:37:26.99	+65:28:20.9	16	64	MW star
D6	07:35:05.74	+65:45:27.4	165	22	Halo
F1	07:35:12.43	+65:43:15.8	210	45	Halo
F16	07:38:01.52	+65:33:00.6	165	43	Disc
JD1	07:37:52.89	+65:34:07.6	145	46	Halo
JD2	07:33:34.58	+66:56:29.8	0	12	MW star
JC15	07:36:18.55	+65:38:33.0	96	8	Disc
F46	07:36:29.16	+65:40:33.5	140	–	Halo

Note. RV and S/N per Å are measured from our KCWI spectra. The RV of F46 was measured from a HIRES spectrum by L21. Typical velocities uncertainties are on the order of 10 km s^{-1}.

cubes and cropped them to the wavelength range common to all slices to use them for the remainder of our analysis. The GCs were sky subtracted by taking an appropriately sized region centred on each cluster and subtracting off an on-chip offset region as 'sky'. Where multiple exposures were taken on the same object these were mean stacked to produce a single spectrum for each GC. Final integration times for each object were: 1440 s for C1, 2400 s for C4, 1200 s for D02, 1200 s for D06, 1200 s for F1, 1440 s for F16, 1200 s for JD1, 900 s for JD2, and 900 s for JC15.

Table 2 lists the candidate coordinates, signal-to-noise ratio of each spectrum and our measured radial velocity (RV) (with a barycentric correction applied) with typical uncertainties of $\sim$10 km s^{-1}. All of the measured radial velocities are consistent with those expected from NGC 2403; however, they are also within the velocity range of Milky Way stars.

The GC candidates shown in Fig. 3 are colour coded according to their measured RV. The general rotation of the stellar and HI disc from Fraternali et al. (2002) shows that the SE side of NGC 2403 is receding at 250 km s^{-1} while the NW side is 'approaching' us at 10 km s^{-1} (the maximum disc rotation velocity is around 130 km s^{-1}). The mean RV of NGC 2403 is 133 km s^{-1}. On the basis of measured velocities relative to the galaxy's velocity field, we suggest that D6, F1, and JD1 (and F46) are GCs likely associated with the halo rather than the disc of NGC 2403. Given that these GCs all lie within a projected distance of 13 kpc, they may be more akin to *inner* halo GCs as seen in the Milky Way's GC system. The objects consistent with the general disc rotation are C1, C4, F16, and JC15.

Although the dwarf galaxy DDO 44 reveals a tidal stream due to likely interaction with NGC 2403 (Carlin et al. 2019) it has a RV of 255 km s^{-1} and so JD2 with a velocity of $\sim$0 km s^{-1} is very unlikely to be associated with DDO 44. We conclude that JD2 is a likely foreground star. Candidate D2 has a blue colour, a near zero radial velocity, and a similar flux in 3 and 12 pixels in our HSC imaging and *Gaia* parameters consistent with a Milky Way star. So, despite the extended size for D2 given by Davidge (2007), we conclude that it is actually a foreground star.

The status of each GC candidate is summarized in Table 2, with seven being confirmed GCs and two as foreground stars. We will therefore no longer consider these stars further. Fig. 4 shows the KCWI spectra for the final sample of seven confirmed GCs (and highlights the different wavelength scales used for the observations). The key absorption lines are indicated.

4 STELLAR POPULATION ANALYSIS

To analyse the stellar populations of the seven GCs, we follow the method outlined in Ferré-Mateu et al. (2021) for compact stellar systems. Briefly, we use the MILES SSP library (Vazdekis et al. 2010) models with the BaSTI isochrones, considering templates that range from metallicities of [Z/H] $= -2.42$ to $+ 0.40$ dex and that cover ages from 0.03 to 14 Gyr, assuming a universal Kroupa IMF. The SSP models include different alpha element ratios, from solar to super-solar (Vazdekis et al. 2016). The work of Mendel, Proctor & Forbes (2007) compared the SSP models of Vazdekis et al. (2016) to other SSP models and found good consistency for Milky Way GCs. We run pPXF using multiplicative polynomials and applying a regularization value that ensures that the resulting star formation history is the smoothest possible while maintaining a realistic fit. The best-fitting SSP model using pPXF (Cappellari 2012) for each GC is overplotted in Fig. 4. For the results, we adopt the means of the mass-weighted stellar population parameters. However, for the [Fe/H] metallicity that is measured directly from the absorption line indices. For the [α/Fe] ratios we employ the Mg$_b$ and Fe5015 lines (which are common to all spectra; these same pairs were employed by the SAURON survey of early-type galaxies; Peletier et al. (2007)). We find that only JD1 has a clear super-solar alpha element enhancement and, in this case, we employ the corresponding alpha-enhanced, rather than base, MILES models. Otherwise, the GCs are consistent with a solar alpha element ratio.

Table 3 presents the mean mass-weighted stellar populations that we measure for the ages and metallicities with uncertainties. Quoted uncertainties are determined using a Monte Carlo technique in which we have varied different ingredients in the pPXF analysis, (e.g. polynomials, degree, regularization, alpha versus base models) to determine the overall uncertainties. Stellar masses are calculated from g-band magnitudes and the resulting mass-to-light ratio from the SSP analysis. We note the very young age of the cluster C1 (400 Myr) and the strong Balmer absorption lines in its spectrum. Our SSP analysis reveals no evidence for a hidden old stellar population

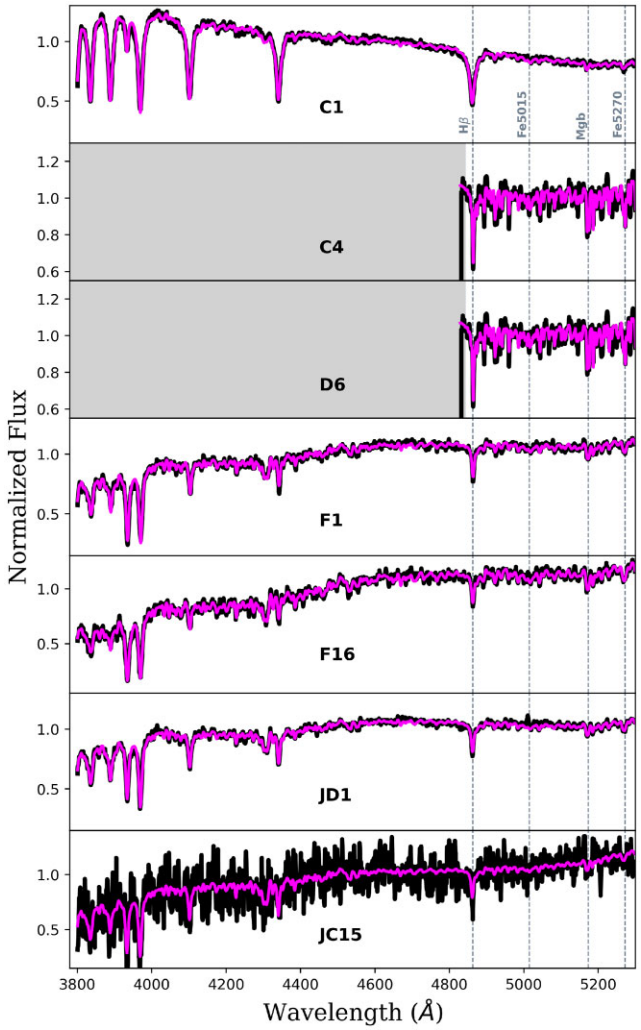

Figure 4. KCWI spectra for each confirmed GC as labelled. Original spectra, shifted to rest wavelength, are shown in black and our model fits in magenta. The key absorption lines used for the analysis are shown in vertical lines (e.g. H β, Fe5015, Mgb, and Fe5270), as labelled in the top panel. Note that different KCWI grating setups were used in the observations, and thus the grey area corresponds to wavelengths not covered by the shorter grating, the BH3.

Table 3. NGC 2403 GC Stellar Populations.

ID	Age (Gyr)	[Z/H] (dex)	[Fe/H] (dex)	M_* (10^5 M$_\odot$)
C1	0.4 ± 0.2	–0.61 ± 0.29	–0.4 ± 0.50	0.5
C4	12.5 ± 1.6	–2.07 ± 0.18	–2.20 ± 0.15	12
D6	7.8 ± 1.5	–1.25 ± 0.04	–1.20 ± 0.15	2.8
F1	9.0 ± 2.9	–1.25 ± 0.20	–1.35 ± 0.30	5.0
F16	9.3 ± 2.2	–0.71 ± 0.29	–1.15 ± 0.20	4.1
JD1	8.6 ± 2.9	–1.24 ± 0.31	–1.60 ± 0.30	4.5
JC15	10.8 ± 2.1	–1.41 ± 0.28	–1.50 ± 0.20	2.9
F46	≤13	–	–1.70 ± 0.03	11

Note. See text for details of possible systematic effects on stellar population parameters. F46 measured from a HIRES spectrum by L21.

for this GC. Although we continue to refer to C1 as a GC, some prefer the 'young massive cluster' nomenclature.

For F46, we list the stellar population parameters determined independently by L21, i.e. their assumed age and measured [Fe/H] metallicity (they found [α/Fe] = +0.15). Their assumed age, of 13 Gyr, can be considered an upper limit. For the stellar mass, we assume the same ratio as JC15 (i.e. M/L$_g$ ∼ 2), which gives a stellar mass of 11 × 10^5 M$_\odot$ in reasonable agreement with the dynamical mass calculated by L21 of 15 × 10^5 M$_\odot$.

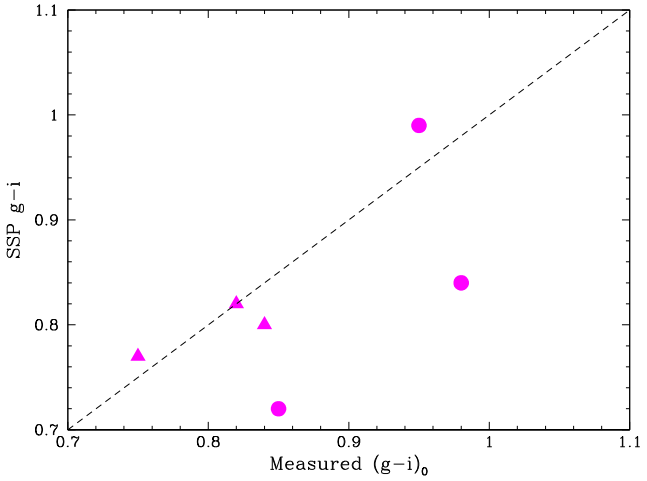

Figure 5. Comparison of $g - i$ colours predicted from our single stellar population (SSP) analysis versus the observed colours (corrected for Galactic extinction) for NGC 2403 GCs. Magenta filled circles show disc GCs and filled triangles show inner halo GCs. The plot focuses on the old, red GCs: the young blue cluster C1 (with SSP $g - i$ of 0.2 and observed $g - i$ of 0.15) is not shown. The dashed line shows a one-to-one line. Corrections for internal extinction would move data to bluer observed colours.

Using the stellar parameters determined from our SSP analysis, we predict $g - i$ colours for our GCs. These predicted colours are compared to the measured colours, corrected for Galactic extinction (A$_V$ = 0.11), in Fig. 5. The predicted and Galactic extinction-corrected colours are in reasonable agreement, thus providing further confidence in our stellar population analysis. Correction for internal dust extinction within NGC 2403 for the disc GCs could improve the agreement further.

Before discussing our stellar population results, it is worth reviewing the potential biases and caveats in the object selection and data analysis. Both the literature and our own selection of GC candidates are naturally biased away from the inner disc due to the possible confusion with young star clusters and H II regions. This might tend to bias our sample against the selection of metal-rich disc GCs.

The stellar masses calculated for our sample of GCs (see Table 3) are all but one above 10^5 M$_\odot$. With a mean GC mass of around 2 × 10^5 M$_\odot$ for the Milky Way's GC system, this indicates that our sample is drawn from the most massive or brightest (for comparison, the GC turnover magnitude is M$_g$ ∼ −7.2) of the GCs in NGC 2403. We note that selecting the more massive GCs from the Milky Way's system would create a bias towards selecting accreted GCs (Mackey & van den Bergh 2005).

There is the possibility of contamination in our GC spectra by emission lines associated with star formation in the disc of NGC 2403. If present, H β emission would tend to fill in the H β absorption line resulting in an older inferred age if not corrected for. If contamination from emission lines was present, we would expect to see the [O III] line at 5007 Å – a visual inspection reveals no clear evidence for [O III]. Furthermore, there is no evidence for emission lines from our pPXF analysis of the entire spectrum. Thus, we conclude that our spectra do not suffer from such contamination.

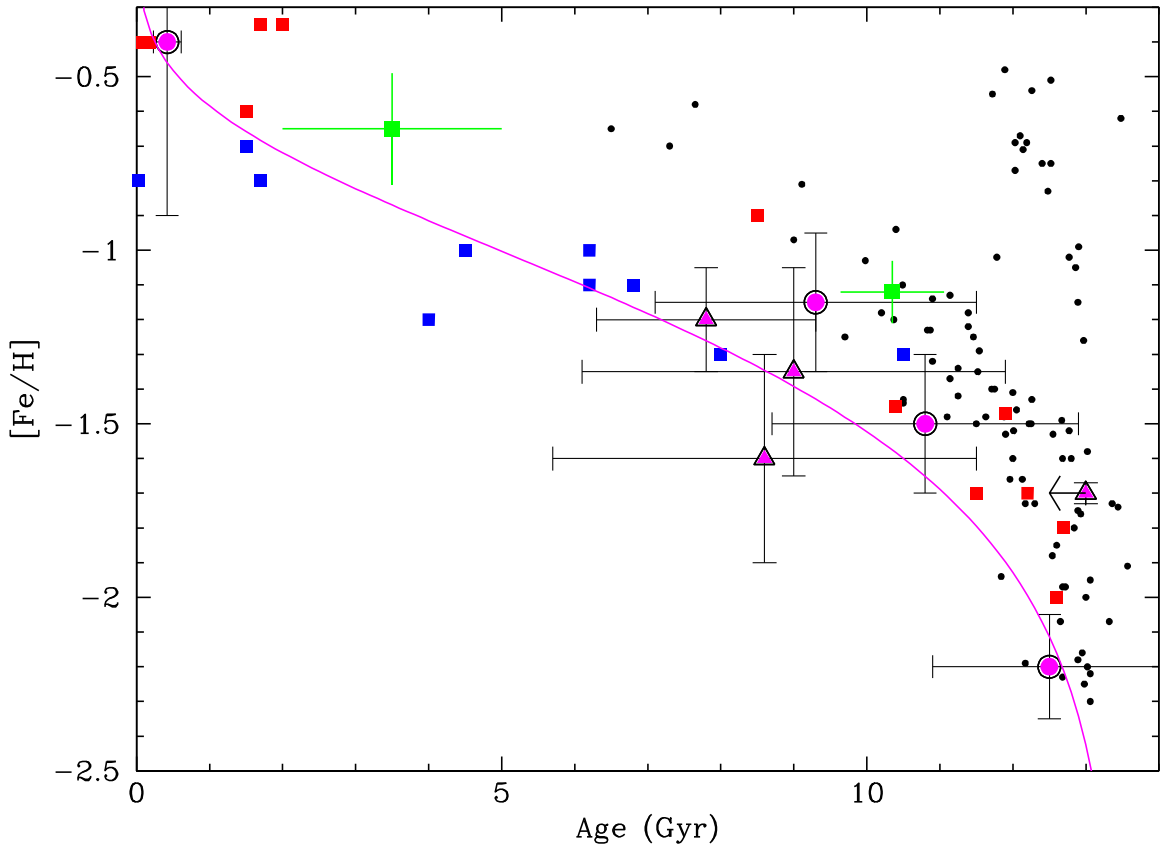

Figure 6. Age-metallicity relation (AMR) for NGC 2403 GCs. Magenta filled circles show NGC 2403 disc GCs and filled triangles show inner halo GCs. For GC F46, an age of 13 Gyr was assumed in L21. The green squares with error bars show an intermediate-age GC and the mean value for several outer halo GCs in M33. Red and blue squares (without error bars) show a selection of LMC and SMC GCs, respectively, with reliable ages and metallicites. Small black circles show Milky Way GCs. The magenta line shows a representative chemical enrichment model for the NGC 2403 GCs. The NGC 2403 GCs are more metal-poor on average at a given age than those in the Milky Way but similar to those in the SMC.

Moreover, the observed GCs may contain blue horizontal branch (BHB) stars. These hot stars can give the impression of a young spectral age while having a limited effect on the derived metallicity and alpha elements (Conroy et al. 2018). The study by Mendel et al. (2007) examined the effects of BHB stars on the derived stellar population parameters from integrated spectra and found a limited impact when a large spectral range was used. We thus consider that the ages of those GCs with a shorter baseline should be considered lower limits, as without higher quality and/or longer baseline spectra, we are unable to rule out the presence of BHB stars.

5 RESULTS AND DISCUSSION

In this work, we obtain spectra, radial velocities, stellar population parameters (age, metallicity, and alpha abundances) and stellar masses for seven confirmed GCs associated with NGC 2403. One additional GC, F46, was previously observed using HIRES at the Keck Observatory by L21, and we included it in our subsequent analysis. They derived a radial velocity (confirming association with NGC 2403), a low metallicity, and a mildly enhanced alpha element ratio. Previously, Battistini et al. (1984) managed to obtain low-quality spectra of three GC candidates (C3, C4, and F21). For C3, they noted similarities to an A-type spectrum, indicating an age of around $\leq$1 Gyr. For the only object in common with this study, C4, they described the spectrum as being that of a classical GC (which we confirm). For F21, they concluded that it was a background galaxy.

The stellar populations, and possible biases/caveats, for the Keck-observed GCs are summarized in Section 4 and Table 3. Bearing in mind that eight GCs out of a possible GC system of around 50 may not be representative, we discuss our sample of high-mass disc/halo GCs in the context of GC systems in other nearby galaxies below.

Our data indicate that the GC system of NGC 2403 was formed over an extended period of time from early in the Universe until today. The GCs have near solar alpha-element ratios with one presenting super-solar enhancement. Compared to the two subpopulations of the Milky Way's GC system, the old GCs studied here are all relatively metal-poor ([Fe/H] ≤ -1); only the very young cluster C1 is metal-rich. We note that Davidge (2003) also measured a low metallicity of [Fe/H] $= -2.2$ for field stars in the outer halo (projected $\sim$22 kpc along the minor axis, beyond our most distant GC) of NGC 2403. This metallicity is comparable to that for the oldest GCs in our sample.

In Fig. 6, we show the ages and [Fe/H] metallicities for our NGC 2403 GCs, along with those of the Milky Way, the Magellanic Clouds, and M33 (a possible analogue galaxy to NGC 2403). For M33, we show a confirmed intermediate-aged (2–5 Gyr) GC from (Chandar et al. 2006) which has a metallicity of [Fe/H] $= -0.65 \pm 0.16$ (Sarajedini et al. 2000). We also show the mean values for a dozen old M33 GCs (i.e. age $= 10.35 \pm 0.71$ Gyr and [Fe/H] $= -1.12 \pm 0.09$) from Beasley et al. (2015). We refer the reader to L21 for arguments

that some of the Beasley et al. (2015) objects may actually be foreground stars (their exclusion does not significantly change the mean values). For the Magellanic Clouds, we take the reliable ages and metallicities from the appendix of Horta et al. (2021), i.e. those with a confidence code of 1. We take ages and metallicities for Milky Way GCs from Forbes (2020). In the Milky Way, the *in situ* formed bulge and disc GCs formed over a short time period (1–2 Gyr) at early times (∼13 Gyr ago), whereas the younger GCs are all the result of *ex situ* formation and subsequent accretion of their host dwarf galaxy (Forbes 2020).

Our observed NGC 2403 GCs in Fig. 6 are coded by whether we have assigned them to the halo or to the disc of NGC 2403 on the basis of their relative velocities (see Table 2). We find no clear distinction between disc and halo GCs in terms of their average age or metallicity. The (disc) GC F46 is shown with an upper age limit of 13 Gyr as assigned by L21. Given that NGC 2043 has little or no bulge (similar to M33), we do not expect bulge GCs to be present, as they are in the Milky Way. At a given age, the NGC 2403 GCs observed in this study have metallicities most similar to those of the SMC, slightly less than those of M33 and the LMC, and systematically lower than GCs accreted from dwarf galaxies on to the Milky Way. In terms of the age distribution, the Magellanic Clouds, M33 and NGC 2403 all appear to have formed star clusters from early times (∼13 Gyr ago) until just a few Gyr ago. We remind the reader of C3 in NGC 2403, which Battistini et al. (1984) claimed has an A-type spectrum indicative of a ≤1 Gyr old GC. Furthermore, massive (∼10^5 $M_\odot$), young (∼0.1 Gyr) star clusters have been identified by Larsen & Richtler (1999) to be forming up to the present day in NGC 2403.

To further discuss the age-metallicity distribution of our observed GCs, we also show in Fig. 6 the AMR for a leaky-box chemical enrichment model. The chemical enrichment models assume non-enriched gas 13.5 Gyr ago and an effective yield of p (i.e. elements returned to the ISM for subsequent star formation after accounting for outflows of enriched material), which is related to stellar metallicity by the equation:

$$[\mathrm{Fe/H}] = -p \ln (t/13.5)$$

Such a model provides a good representation for the GCs from disrupted satellites in the Milky Way. Indeed, this aspect of dwarf galaxy GC systems was used by Kruijssen et al. (2019) and Forbes (2020) to associate individual Milky Way GCs with disrupted satellites. The yields for the five largest disrupted satellites, including the Sgr dwarf, were found to range from 0.22 to 0.35. The model shown in Fig. 6 has $p = 0.1$ and is very similar to the one derived from the stars in the SMC ($M_* = 0.4 \times 10^9 M_\odot$) by Leaman, VandenBerg & Mendel (2013).

The steepness of an AMR (i.e. the metallicity at a given age), as represented by the yield, is primarily driven by the mass of the host galaxy. Given that the AMR for NGC 2403 appears to be lower than that of dwarf galaxies accreted on to the Milky Way and perhaps also the GCs of M33 (which has a similar luminosity to NGC 2403), other factors could be at play. One factor that may act to lower an AMR is the outflow of enriched material. In a study of nearby spirals and dwarf galaxies, Dalcanton (2007) concluded that *'Metal-enriched outflow is therefore the only viable mechanism for producing galaxies with low effective yields.'* The presence of an extended 'HI halo' around NGC 2403 led Fraternali et al. (2002) to suggest that it may be the signature of a galactic fountain. This outflow from the disc to the halo may contribute to the low effective yield as argued by Dalcanton (2007). Furthermore, there is a step change in the effective yield to lower values at rotation speeds of $V_{\rm rot} \leq 150$ km s^{-1} (Garnett 2002). NGC 2043, with $V_{\rm rot} \sim 130$ km s^{-1} falls close to this key transition.

Cosmological simulations predict that galaxies of NGC 2403's mass have not undergone significant accretion (e.g. in the model of Choksi & Gnedin (2019)) and only *in situ* formed GCs are expected. Indeed, there are several arguments against NGC 2403 having experienced a massive merger event in the past, which would mean few, if any, accreted GCs. NGC 2403 is relatively isolated and may only be infalling into the low mass M81 group for the first time (there is no evidence of ram pressure stripping). It also reveals a remarkably uniform, regularly rotating HI disc (de Blok et al. 2008). Its old stellar disc has a uniform metallicity of [Fe/H] ∼ −1 (consistent with our most metal-rich GCs), indicating that it is well-mixed, and has an unbroken surface brightness profile (Williams et al. 2013). This suggests a relatively undisturbed galaxy despite its probable interaction with the dwarf satellite DDO 44 (Carlin et al. 2021). Davidge (2003) found evidence for AGB stars (ages ≤ 1 Gyr) beyond the disc of NGC 2403 and argued that they formed *in situ* and not from accretion. We also note that F46 does not have the anomalous chemical signature indicative of an accreted GC (L21). While we cannot rule out accreted GCs, our sample of GCs is likely formed, over many Gyr, from *in situ* gas.

6 CONCLUSIONS

In this work, we studied a sample of relatively high-mass GCs associated with the low mass, bulgeless galaxy NGC 2403. Based on GC candidates in the literature, and new candidates selected from SDSS and our (HSC) imaging, we obtained spectra of nine candidates using the KCWI instrument at the Keck Observatory. We confirm seven of them to be GCs associated with NGC 2403, with the remaining two likely to be foreground stars. Our results are supplemented with one additional GC observed using HIRES, also from Keck, by L21.

By comparing the radial velocities of the eight confirmed GCs with the overall rotation of the HI disc, we assign four GCs to the disc and four to the halo. Single Stellar Population (SSP) model fits indicate that the GCs were formed over many Gyr (with the caveat that the presence of blue horizontal branch stars can make GCs appear much younger than they are). We find most to be consistent with solar alpha element ratio. However, the old GCs are all found to be metal-poor, i.e. [Fe/H] ≤ −1. The one young, massive cluster we obtain a spectrum for is more metal-rich. Cosmological simulations predict that few, if any, accreted GCs will be found in galaxies of the mass of NGC 2403. Based on the lack of disturbance in the stellar and HI disc, and its relative isolation, both the disc and halo GCs of NGC 2403 likely formed over an extended period from *in situ* gas.

Our NGC 2403 GCs are systematically lower in metallicity at a given age compared to the Milky Way's GC system and perhaps also to the GCs in M33. However, they exhibit a similar AMR to the GCs of the Small Magellanic Cloud. The AMR of the NGC 2403 GCs can be approximated by a leaky-box chemical enrichment model with a similar effective yield than that inferred for the SMC stars. Outflows of enriched material may explain the relatively low yield inferred for NGC 2403's GC system.

ACKNOWLEDGEMENTS

We thank. S. Larsen for supplying information regarding the GC F46 prior to publication and for his comments on our paper. We thank the MADCASH team for the original HSC observations and D. Sand for his comments. We thank the referee for several suggestions that have

improved this paper. AFM has received support from the Severo Ochoa Excellence scheme (CEX2019-000920-S) and through the Postdoctoral Junior Leader Fellowship Programme from 'La Caixa' Banking Foundation (LCF/BQ/LI18/11630007). AJR was supported by the National Science Foundation grant AST-1616710 and as a Research Corporation for Science Advancement Cottrell Scholar. JLC acknowledges support from National Science Foundation grant AST-1816196.

This work was supported by a NASA Keck PI Data Award, administered by the NASA Exoplanet Science Institute. Data presented herein were obtained at the W. M. Keck Observatory from telescope time allocated to the National Aeronautics and Space Administration through the agency's scientific partnership with the California Institute of Technology and the University of California. The Observatory was made possible by the generous financial support of the W. M. Keck Foundation. The authors wish to recognize and acknowledge the very significant cultural role and reverence that the summit of Maunakea has always had within the indigenous Hawaiian community. We are most fortunate to have the opportunity to conduct observations from this mountain.

DATA AVAILABILITY

Keck data are available from the Keck Observatory Archive (KOA) at https://www2.keck.hawaii.edu/koa/public/koa.php. Sloan Digital Sky Survey (SDSS) photometry is available at http://skyserver.sdss.org/dr7/en/home.aspx. *HST* data are available from the MAST archive at https://archive.stsci.edu/missions-and-data/hst.

REFERENCES

Barker M. K., Ferguson A. M. N., Irwin M. J., Arimoto N., Jablonka P., 2012, MNRAS, 419, 1489
Battistini P., Bonoli F., Federici L., Fusi Pecci F., Kron R. G., 1984, A&A, 130, 162
Beasley M. A., San Roman I., Gallart C., Sarajedini A., Aparicio A., 2015, MNRAS, 451, 3400
Burkert A., Forbes D. A., 2020, AJ, 159, 56
Cappellari M., 2012, Astrophysics Source Code Library, record ascl:1210.002
Carlin J. L. et al., 2016, ApJ, 828, L5
Carlin J. L. et al., 2019, ApJ, 886, 109
Carlin J. L. et al., 2021, ApJ, 909, 211
Chandar R., Bianchi L., Ford H. C., Sarajedini A., 2002, ApJ, 564, 712
Chandar R., Puzia T. H., Sarajedini A., Goudfrooij P., 2006, ApJ, 646, L107
Choksi N., Gnedin O. Y., 2019, MNRAS, 488, 5409
Conroy C., Villaume A., van Dokkum P. G., Lind K., 2018, ApJ, 854, 139
Dalcanton J. J., 2007, ApJ, 658, 941
Davidge T. J., 2003, AJ, 125, 3046
Davidge T. J., 2007, ApJ, 664, 820
de Blok W. J. G., Walter F., Brinks E., Trachternach C., Oh S. H., Kennicutt R. C. J., 2008, AJ, 136, 2648
Fan Z., de Grijs R., 2014, ApJS, 211, 22
Ferré-Mateu A., Durré M., Forbes D. A., Romanowsky A. J., Alabi A., Brodie J. P., McDermid R. M., 2021, MNRAS, 503, 5455
Forbes D. A. et al., 2018, Proc. R. Soc. A, 474, 20170616
Forbes D. A., 2020, MNRAS, 493, 847
Forbes D. A., Remus R.-S., 2018, MNRAS, 479, 4760
Fraternali F., van Moorsel G., Sancisi R., Oosterloo T., 2002, AJ, 123, 3124
Gaia Collaboration et al., 2016, A&A, 595, A1
Gaia Collaboration et al., 2021, A&A, 649, A1
Garnett D. R., 2002, ApJ, 581, 1019
Gilbert K. M. et al., 2022, ApJ, 924, 116
Harris W. E., Harris G. L. H., Alessi M., 2013, ApJ, 772, 82
Horta D., Hughes M. E., Pfeffer J. L., Bastian N., Kruijssen J. M. D., Reina-Campos M., Crain R. A., 2021, MNRAS, 500, 4768
Hughes A. K. et al., 2021, ApJ, 914, 16
Kruijssen J. M. D., Pfeffer J. L., Crain R. A., Bastian N., 2019, MNRAS, 486, 3134
Larsen S. S., Richtler T., 1999, A&A, 345, 59
Larsen S. S., Eitner P., Magg E., Bergemann M., Moltzer C. A. S., Brodie J. P., Romanowsky A. J., Strader J., 2021, preprint (arXiv:2112.00081) (L21)
Leaman R., VandenBerg D. A., Mendel J. T., 2013, MNRAS, 436, 122
Li P., Lelli F., McGaugh S., Schombert J., 2020, ApJS, 247, 31
Lira P., Johnson R. A., Lawrence A., Cid Fernandes R., 2007, MNRAS, 382, 1552
Lomelí-Núñez L., Mayya Y. D., Rodríguez-Merino L. H., Ovando P. A., Rosa-González D., 2022, MNRAS, 509, 180
Lynden-Bell D., Lynden-Bell R. M., 1995, MNRAS, 275, 429
Mackey A. D., van den Bergh S., 2005, MNRAS, 360, 631
Mendel J. T., Proctor R. N., Forbes D. A., 2007, MNRAS, 379, 1618
Morrissey P. et al., 2018, ApJ, 864, 93
Oser L., Ostriker J. P., Naab T., Johansson P. H., Burkert A., 2010, ApJ, 725, 2312
Peletier R. F. et al., 2007, MNRAS, 379, 445
Remus R.-S., Forbes D. A., 2021, preprint (arXiv:2101.12216)
Saha A., Thim F., Tammann G. A., Reindl B., Sandage A., 2006, ApJS, 165, 108
San Roman I., Sarajedini A., Aparicio A., 2010, ApJ, 720, 1674
Sarajedini A., Geisler D., Schommer R., Harding P., 2000, AJ, 120, 2437
Vazdekis A., Sánchez-Blázquez P., Falcón-Barroso J., Cenarro A. J., Beasley M. A., Cardiel N., Gorgas J., Peletier R. F., 2010, MNRAS, 404, 1639
Vazdekis A., Koleva M., Ricciardelli E., Röck B., Falcón-Barroso J., 2016, MNRAS, 463, 3409
Williams B. F., Dalcanton J. J., Stilp A., Dolphin A., Skillman E. D., Radburn-Smith D., 2013, ApJ, 765, 120

APPENDIX A: GLOBULAR CLUSTER CANDIDATE IMAGING

Images, from *HST* or SDSS, of our GC candidates studied in this work, along with the confirmed GC (F46) of L21. We find two candidates (D2 and JD2) to be foreground stars.

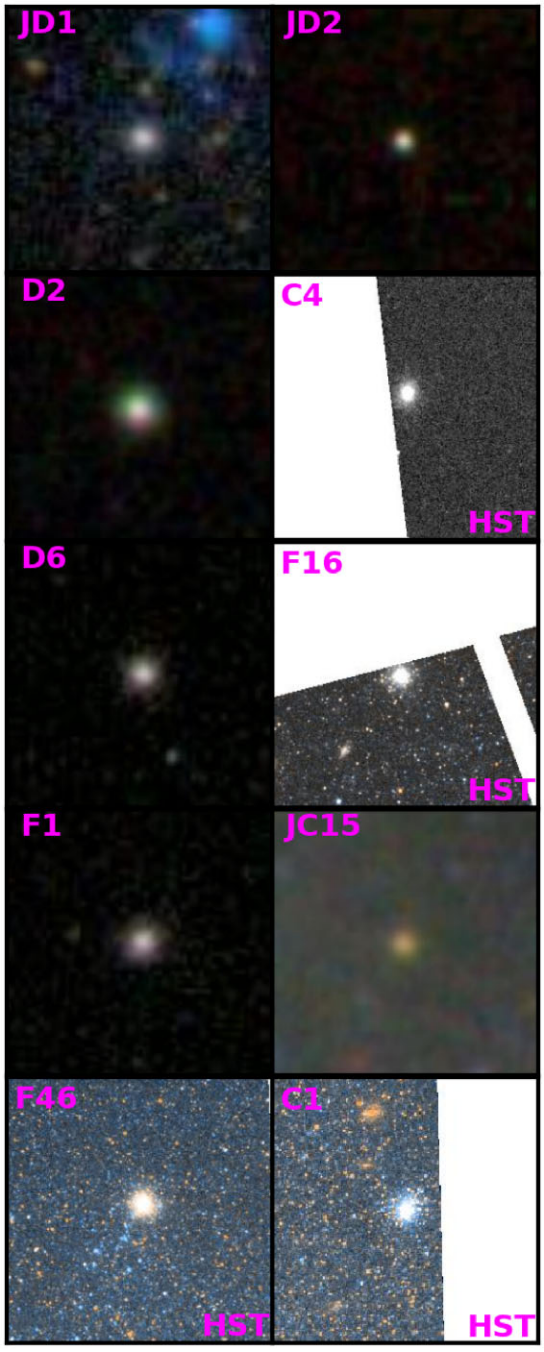

Figure A1. A montage of the GC candidates studied in this work is taken from SDSS or, if available, from *HST* imaging. GC IDs are labelled. Each image postage stamp covers a field of view of 25.6 × 25.6 arcsec^2. At 3.2 Mpc, 1 arcsec = 15 pc. We conclude that D2 and JD2 are foreground stars (see text for details).

This paper has been typeset from a TEX/LATEX file prepared by the author.